

# How the finite element method helps explaining fatigue crack growth retardation and acceleration

Johan Maljaars <sup>a, b</sup>, Lisa Tang <sup>a</sup>

<sup>a</sup> TNO, the Netherlands

<sup>b</sup> Eindhoven University of Technology, the Netherlands

Crack closure effects during fatigue crack growth have been studied by many researchers with the finite element method, but appears difficult to accurately predict. Although quantification of crack closure may be a bridge too far, finite element models may help explaining observations from tests and give insight into trends. This paper studies crack closure resulting from large stress peaks (overloads) and deep valleys (underloads) in a further constant amplitude load. Middle tension and single edge notched specimens of steel and aluminium are simulated. Effects of overloads and of combinations of overloads and underloads for the two geometries and materials are studied and explanations for experimental observations are provided.

*Key words: Retardation, fracture mechanics, plasticity induced crack closure, crack growth acceleration, fatigue, overload effect*

## Nomenclature

Symbols:

$C$	Paris' equation constant
$D$	Ratio between the stress range at over- or underload and constant amplitude stress range
$K$	Stress intensity factor
$N$	Number of cycles
$R$	Stress ratio, i.e. ratio between minimum and maximum stress of a cycle
$R_{inf}$	Maximum change in yield surface size
$S$	Stress
$S_0$	Yield surface size

$S_{res}$	Residual stress
$S_y$	Yield surface size at zero plastic strain
$U$	Ratio between effective and total stress (intensity factor) ranges
$W$	MT specimen width or SENB4 specimen height
$X$	Back stress
$Y$	Geometric correction factor
$\Delta$	Range operator
$\Delta K_{th}$	Threshold stress intensity factor
$a$	(Semi) crack length
$b$	Rate at which the yield surface size changes
$m$	Paris' equation exponent
$\beta$	Maximum change of back stress
$\bar{\epsilon}_{pl}$	Equivalent plastic strain
$\gamma$	Rate at which back stress changes

Subscripts:

est	Estimate
max	Maximum value
min	Minimum value
open	At opening of the crack
OL	At application of an overload
UL	At application of an underload
eff	Effective

Abbreviations:

CA	Constant amplitude
FEM	Finite element method
GP	Gauss point
IP	Integration point
MT	Middle-tension specimen
OL	Overload
PICC	Plasticity-induced crack closure
SENB4	Single-edge notched specimen loaded in 4-point bending
UL	Underload

# 1 Introduction

Many tests described in literature indicate that fatigue crack growth is retarded after the application of a large stress peak (referred to as overload or OL) in a further constant amplitude (CA) loading. Although the general consequences of OL-s have been experienced under many conditions, tests indicate that the amount of retardation depends on the material type and geometry: Aluminium alloys are known for their different crack growth retardation behavior than steels, e.g. [1]-[3] and retardation is larger in specimens in an almost plane stress state as compared to an almost plane strain state, e.g. [4]-[6]. It is also known that a deep stress valley (referred to as underload or UL) can cause crack acceleration [7]-[9]. The combined effects of OL-s and UL-s on the crack growth rate in a variable amplitude spectrum appears to be different from the arithmetic sum of retardation and acceleration effects of individual OL-s and UL-s [10]-[12]. To date, a sound explanation has not been found for these experimental observations.

Although continuous debate amongst researchers exists on the physical explanation ([13]-[15]), most researchers agree that contact of the crack flanks near the crack tip during a portion of the stress cycle plays an important role in the retardation effect in plane stress of metals, [16]. The large plastic strains in the process zone at the crack tip are considered being responsible for crack flank contact, Figure 1. The stretched material along the crack flanks acts as a wedge and prevents complete closure of the crack. An OL results in a larger plastic zone as compared to a small stress cycle. As a result, the stress level required to open the crack in stress cycles following an OL is larger as compared to the same cycle before the OL application.

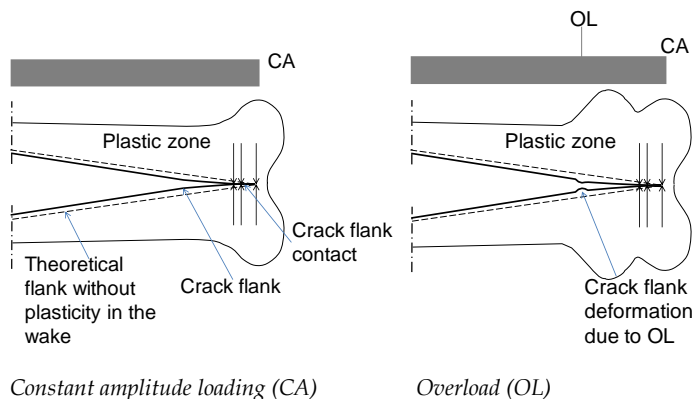


Figure 1: Theoretical crack closure concept

The plasticity induced crack closure (PICC) concept is more ambiguous for a plane strain state. Whereas the extra material in the wake required for PICC may originate from the thickness direction in plane stress, this source of material is not available for a plane strain condition. Many researchers therefore believe that crack closure cannot occur in plane strain. In addition, tests on increasingly thick specimens in [17] provide a decreasing amount of crack closure. Using a three-dimensional numerical model of a thick-walled body with a straight crack front, [18] demonstrates that plastic stretching of material mainly occurs at the edges, where a plane stress condition applies. Similar results were obtained in [19]-[20]. Several researchers have studied crack closure with two-dimensional plane strain models, with different results. Significant crack closure levels were reported in [21]-[23] whereas [24] reports that a crack opens already at the minimum stress of a cycle. Ratcheting of the material at the crack tip may be more important in case of plane strain as compared to plane stress, [25].

The aim of the current paper is to fund explanations for differences in crack closure and crack growth rate variations caused by OLs and ULs by employing the finite element method (FEM).

## 2 A critical review of crack closure evaluation models

Possibilities of modelling fatigue crack growth in FEM are using cohesive zones, e.g. [26], or the thick level set [27]. The crack tip does not have a discrete location in these models. Instead, a gradual debonding of the nodes at both crack flanks is modelled over a certain length in the vicinity of the crack tip. This paper, however, considers another option, where a body including a crack is taken as starting point. The actual crack growth process due to cyclic loading is not modelled. Instead, several load cycles are applied so that a plastic field is formed. Subsequently the constraint at the crack tip node is released so that the new crack tip is located one node further along the predefined crack path (Figure 2). This is repeated until a stable plastic region is obtained in the wake. The far field stress is determined at which the crack opens,  $S_{open}$ . In the crack closure concept, the effective stress range is considered as the difference between maximum stress and the opening stress and the stress range effectivity ratio,  $U$ , is defined as ratio between the effective part of the cycle and the total cycle:

$$U = \frac{S_{\max} - S_{\text{open}}}{S_{\max} - S_{\min}} \quad (1)$$

where  $S_{\max}$  and  $S_{\min}$  are the far field maximum and minimum stress of a cycle, respectively. The effective stress intensity factor range,  $\Delta K_{\text{eff}}$ , is considered the driving parameter for crack growth and is obtained through:

$$\Delta K_{\text{eff}} = U(K_{\max} - K_{\min}) \quad (2)$$

Where  $K_{\max}$  and  $K_{\min}$  are the maximum and minimum stress intensity factors of the cycle, respectively. Hence, in the crack closure concept, the driving crack growth parameter can be determined by evaluating  $K_{\max}$  and  $K_{\min}$  from linear elastic fracture mechanics and in addition  $S_{\text{open}}$  from the non-linear FEM analysis. Hence, the purpose of the FEM analysis as applied in the current research is not simulation of fatigue crack growth itself, but the determination of  $S_{\text{open}}$  or, alternatively,  $U$ .

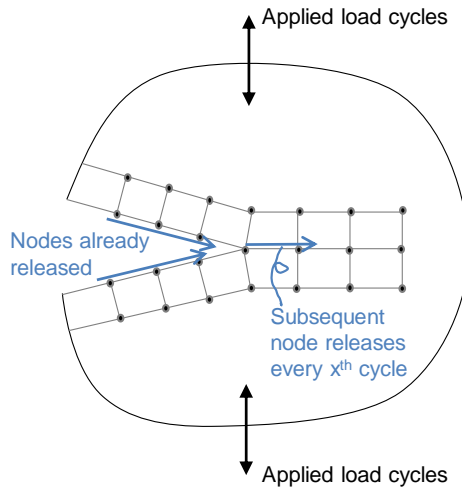


Figure 2: Schematic overview of PICC simulation using subsequent node releases after a certain number of applied load cycles

Simulations of PICC using FEM have been reported in other articles, examples are [21]-[25] and [28]-[30]. Many choices and parameters are involved in simulation of crack closure with FEM. Overviews are given in [31]-[33]. For some of these, experience has resulted in consensus on the best selection. For others – discussed below – it is not straightforward how these should be selected.

An accurate description of the constitutive behavior is a crucial factor in obtaining realistic crack closure results, [33]. Constitutive models that are able to describe both isotropic and kinematic hardening experienced during cyclic loading have provided the most accurate results in [34]. Low cycle fatigue tests are normally carried out to obtain the stabilized stress-strain hysteresis required for setting the parameters of the constitutive model. However, the strain at which the load reversal should take place in the test to represent the state at an advancing crack tip is not well established. In a fatigue loaded body, the material at a certain location in front of the crack tip experiences an increasing strain at load peaks as the crack advances and the distance between the location and the crack tip decreases. Especially in the fatigue process zone – where plastic strain reversal takes place – strains are large and the increase in strain at each (few) load cycle(s) may be significant as the crack grows. Hence, the strain hysteresis may not be stabilized in that case. Constitutive models and test procedures to feed these models so as to accurately model the real behavior are lacking.

The evaluation criterion for crack closure using this method is not straightforward. Methods adopted for determining the crack opening stress are, amongst others, the far field stress at which the first or second node in the wake to the crack tip is no longer in contact [35], the far field stress at which the total compression force executed by all nodes on the crack flank is zero [36], or the far field stress at which the integration point closest to the crack tip experiences a tensile stress, [22], Figure 3 (top graph). The last mentioned criterion provides the largest crack opening stress, followed by first node contact and second node contact provides the lowest value for  $S_{open}$ . In addition, the user needs to define whether  $S_{open}$  is the far field stress at which the crack opens during loading, or the stress at which the crack closes during unloading. Again, this choice influences the result.

Another difficulty arises in selecting an appropriate mesh size. The mesh should be sufficiently dense as to accurately describe the plastic field around the crack tip. For spanning the zone where plastic strains are experienced both in tension and in compression – the so-called reversed plastic zone – between 2 and 4 elements are recommended in [21], [37], [38], the difference being caused by different constitutive laws applied. The crack tip is a discrete point in these models. If a node is released, the crack advances one element distance, which is significantly larger than the actual crack advancement due to one or a few load cycles. Hence, one node release represents several real crack advancements. This gives rise to the following sub questions:

- At which point during a load cycle should the node at the crack tip be released? This usually is done at maximum or minimum load. The results of the analysis depend on this choice, as will be demonstrated later in this paper.
- How many load cycles should be applied between crack tip node releases? The crack opening stress derived with the FEM tends to a stabilised value after a sufficiently large number of cycles between node releases, Figure 3, and the required number of cycles is strongly related to isotropic hardening. However, it has never been demonstrated whether there indeed exists a stable value, or if the opening stress reduction (or increase) continues but with a smaller change as the number of cycles increases. The number of cycles in between node releases to obtain a sufficiently stabilised value may become larger than the actual number of cycles required for the same crack advancement in a real specimen.

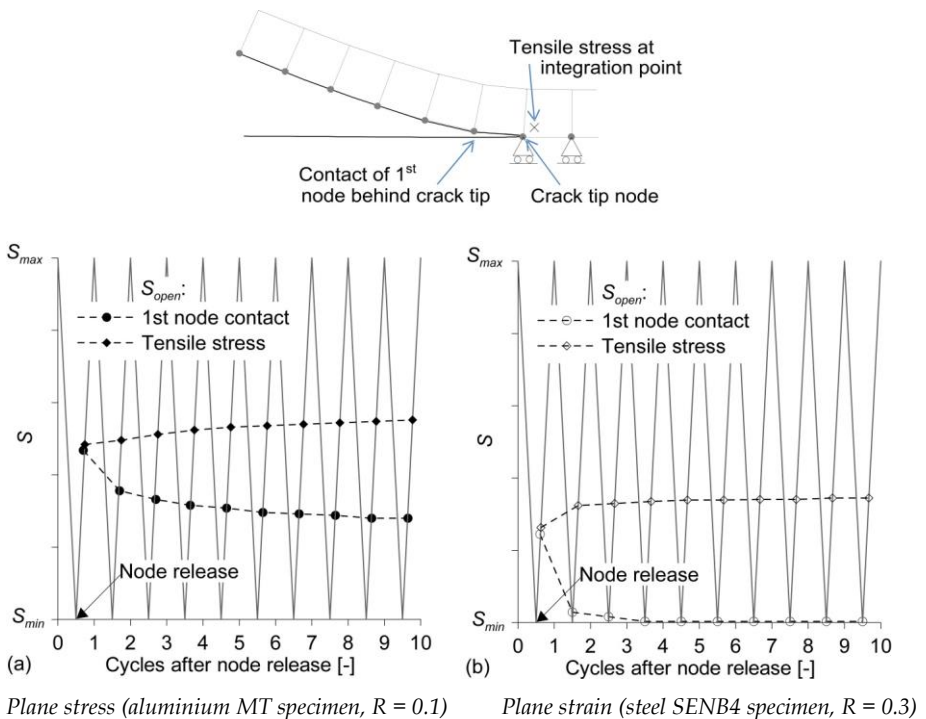


Figure 3: Crack opening stress (presented with dots) at 1 to 10 cycles after node release for constant amplitude loading with the model explained in Section 3

The above points make clear that it is difficult to obtain quantitative values for crack closure using a conventional finite element model. These considerations apply to bodies subjected to constant amplitude loading. For evaluating crack closure after an OL or UL, the criteria are even more troublesome. On the other hand, the FEM can provide a qualitative insight into the physical phenomena responsible for PICC as well as the mechanisms behind crack growth retardation and acceleration after a periodical UL and OL, respectively, by evaluating aspects such as the stress strain hysteresis and the shape of the crack flank. It can therefore help understanding experimental observations.

A number of studies into the effect of OL and block loading on PICC using the FEM have been performed on various metals [7], [36], [39]-[46]. A good agreement was obtained between finite element models and experiments with respect to the predicted and measured crack growth retardation, plastic field, or crack closure, for most of these studies. These studies focused on one specific case i.e. one material and geometry or constraint so that it is difficult to generalize the conclusions. In addition, in most of these studies the material models used consider either kinematic or isotropic hardening – depending on the expected dominant behavior – instead of a combined kinematic and isotropic hardening model. Using the existing crack closure concept with the FEM described above, this paper investigates the physics and compares PICC between steel and aluminium alloys and between plane stress and plane strain, where the effect of OL-s, UL-s, and combinations of OL-s and UL-s on crack closure are studied. With respect to the above-mentioned choices, options are selected that are adopted by most researchers. These are indicated in Table 1.

*Table 1: Evaluation criteria and choices adopted in the FEM*

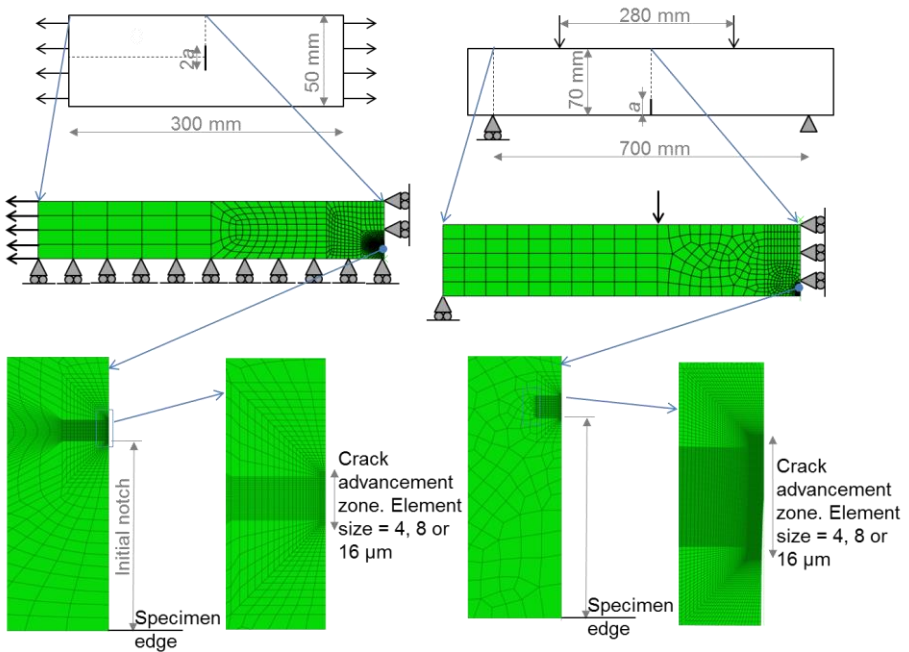
Aspect	Choice
Strain at load reversal	3 %
$S_{open}$ evaluation criterion	Loss of contact of 1 <sup>st</sup> node in the wake
$S_{open}$ evaluation moment	During loading
Mesh size	16 $\mu\text{m}$ <sup>a)</sup>
Node release	At maximum load
# cycles between node releases	2

a) A denser mesh of 8  $\mu\text{m}$  or 4  $\mu\text{m}$  is applied to a selection of the cases to investigate the mesh density sensitivity.

### 3 Description of the numerical model

#### 3.1 Geometry and constitutive law

Four geometries have been modeled using the finite element software Abaqus 6.12-1. A middle tension (MT) specimen (sometimes also referred to as centre-crack specimen in literature) and a single-edge notched specimen loaded in 4-point bending (SENB4) have been modeled with plane stress and plane strain elements (Figure 4). The types of element applied for plane stress and plane strain were CPS4R and CPE4R, respectively, which are four-node elements with reduced integration. The MT specimen size is equal to that in [33] so that results can be compared. The SENB4 specimen size matches that of tests described in [47]. Different crack sizes have been considered and different loads with variations in maximum cyclic stress,  $S_{\max}$ , minimum cyclic stress,  $S_{\min}$ , and stress ratio,  $R = S_{\min} / S_{\max}$ .



(a) Middle tension specimen (MT)

(b) Four-point bending specimen (SENB4)

Figure 4: Specimens and mesh (not on scale)

For reasons of symmetry, only  $\frac{1}{4}$  or  $\frac{1}{2}$  of the geometry has been modeled for the MT and SENB4 specimens, respectively (Figure 4). Square elements were applied in the reversed plastic zone in order to enhance numerical stability, [31]. A mesh refinement was applied near the crack tip with a mesh size of  $16 \mu\text{m}$  for most analyses, so that at least two or more elements were involved in the reversed plastic zone. This mesh may be too coarse for an accurate prediction of PICC levels especially in case of plane strain. Mesh sensitivity was checked for a number of geometries and loading conditions, and the one with the largest mesh sensitivity is depicted in Figure 5. It concerns a plane strain MT specimen of DIN-CK45 steel. Figure 5a demonstrates that the opening stress level increases for an increasingly dense mesh. However, the aim of this study is to investigate trends and to qualitatively determine the effects of OLs and ULs. The interest is therefore in the relative difference between PICC in CA loading and the maximum or minimum PICC after OLs and ULs. Figure 5b indicates that this relative difference is less sensitive to the mesh size.

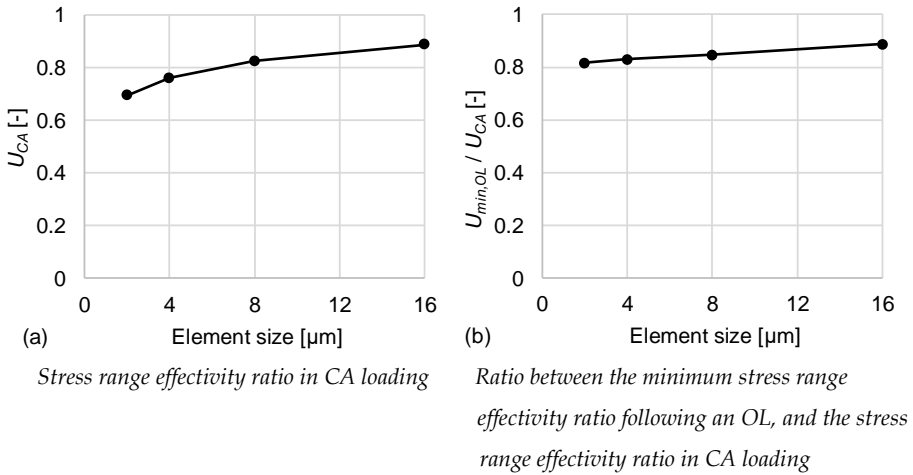


Figure 5: PICC as a function of the element size near the crack tip for a plane strain MT specimen of DIN-CK45 steel with  $S_{\max} = 80 \text{ MPa}$ ,  $S_{\min} = 8 \text{ MPa}$ , and an OL stress of  $SOL = 120 \text{ MPa}$

The combined isotropic and kinematic hardening model applied here is based on Lemaitre and Chaboche, [48]. The isotropic hardening behavior defines the evolution of the yield surface size,  $S_0$ , as a function of the equivalent plastic strain,  $\bar{\epsilon}_{pl}$ , and is given by:

$$S_0 = S_y + R_{\text{inf}}(1 - e^{-b\bar{\epsilon}_{pl}}) \quad (3)$$

where  $S_y$  is the yield surface size at zero equivalent plastic strain,  $R_{inf}$  is the maximum change in the size of the yield surface and  $b$  is the rate at which the size of the yield surface changes as plastic strain increases. The back stress at certain equivalent plastic strain,  $\alpha$ , evolves according to a kinematic hardening rule:

$$\alpha = \beta(1 - e^{-\gamma \bar{\epsilon}_{pl}}) + \alpha_0 e^{-\gamma \bar{\epsilon}_{pl}} \quad (4)$$

where  $\alpha_0$  is the back stress at maximum plastic strain of the stress cycle considered,  $\beta$  is the maximum change of the back stress and  $\gamma$  determines the rate at which the back stress varies with equivalent plastic strain in a stabilized cycle.

The material-dependent parameters  $S_y$ ,  $R_{inf}$ ,  $b$ ,  $\beta$  and  $\gamma$  have been calibrated from cyclic test data described elsewhere for steel grade S355, steel grade DIN-CK45 (comparable to S235) and aluminium alloy AA6061-T4. The parameters in the Chaboche model are a function of the maximum strain of a cycle, [48], and this introduces the difficulty that this maximum strain in fatigue varies: Even in CA loading the maximum strain increases as the distance between the crack tip and the integration point reduces (see also Section 2). The strategy applied in this study is that a first analysis with parameters corresponding to the estimated maximum cyclic strain,  $\epsilon_{est}$ , was carried out and compared with the maximum cyclic strain resulting from the analysis,  $\epsilon_{FEM}$ . A re-run with updated parameters is required if the estimate and the result deviate too much:  $|(\epsilon_{est} - \epsilon_{FEM}) / \epsilon_{FEM}| > 2$ . Table 2 provides the model parameters.

Table 2: Chaboche material parameters used in the analyses

material	$S_y$ [MPa]	$R_{inf}$ [MPa]	$b$ [-]	$\beta$ [MPa]	$\gamma$ [-]	source
alu AA6016-T4	124	291	9.5	34.9	146.5	[33] <sup>a</sup>
steel S355J2H	465	55	2.38	169	139	[49]
steel DIN-CK45	250	50	50	450	175	[50]

<sup>a</sup> Parameters and constitutive model from that source were transformed to match the model provided by Eqs. (3-4).

A certain crack advancement is required for the plastic zone in the wake of the crack to be formed. The required crack advancement for a constant crack opening level and thus a fully developed plastic zone depends on the stress magnitude and the constraint and for the considered cases it varied between 0.3 mm for small stress ranges, low stress ratios and

plane stress conditions to more than 1 mm. All results in this paper are presented after the fully developed plastic zone was obtained.

### 3.2 Crack closure in case of plane strain

A significant difference in crack closure is observed between Figure 3a and Figure 3b. The main cause of this difference is the plane stress versus plane strain constraint. Overviews of the consequences of choices of mesh parameters and evaluation criteria as provided in [31]-[33] are based on plane stress constraint and CA loading. The most important aspects are therefore investigated in this section for plane strain constraints.

In case of the plane strain situation of Figure 3b, the crack opens at minimum stress after a few cycles following the node release. This implies that the full stress cycle is effective, i.e.  $U = 1$ . The number of cycles after which  $S_{\text{open}} = S_{\text{min}}$  depends on the material and stress ratio but in all cases considered ( $R \geq 0.1$ ) this was observed before the 30th cycle after node release. A study into PICC models for the plane strain case is provided in [24] and the same conclusion was obtained there. Based on this, [24] suggests that crack closure is not to be expected in a pure plane strain state for materials exhibiting strong ratcheting. However, that study considered CA loading only. A different situation appears after an overload. Figure 6 provides  $U$  evaluated with Eq. (1) as a function of the number of cycles between node releases before and after the application of an OL. The results before OL are

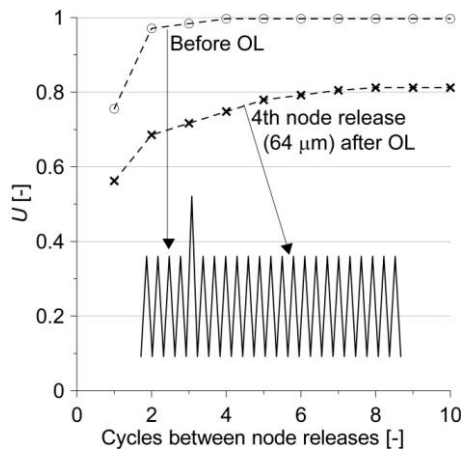


Figure 6: Ratio between effective and total stress intensity factor range,  $U$ , at 1 up to 10 cycles between node releases before and after the application of an overload (OL) for a plane strain steel SENB4 specimen loaded with  $R = 0.3$

equal to those of Figure 3b and indicate that the entire stress range is effective. The results after OL, however, show a reduction of the effective stress ratio. These results indicate that PICC following an OL may occur even if the full cycle is effective before the OL and even in case of plane strain. Analytical retardation models such as [51], [52] and strip yield models fail to describe this case.

A more detailed evaluation of this case is presented in Figure 7, which provides the crack flank position at minimum and maximum load of the simulation of Figure 6 in CA, i.e. before the OL was applied. The crack flank position is plotted after application of the second and tenth cycle following a node release. Before application of the OL - i.e. at CA loading (Figure 7a) only the position of the first node behind the crack tip changes with increasing number of cycles. The opening at this node increases with increasing number of cycles and only for the second cycle the position of this node is in line with the other nodes. In addition, a subsequent node release - i.e. a crack advancement - instantaneously brings the node in line with the other nodes. According to [24] this observation is independent of the mesh density, i.e. also for a denser mesh only the node closest to the crack tip shows this movement as the number of cycles increases. Contact of the first node in the wake of the crack may therefore not be the most optimal criterion for crack closure in plane strain. An alternative evaluation method for closure is extrapolation of the opening of a number

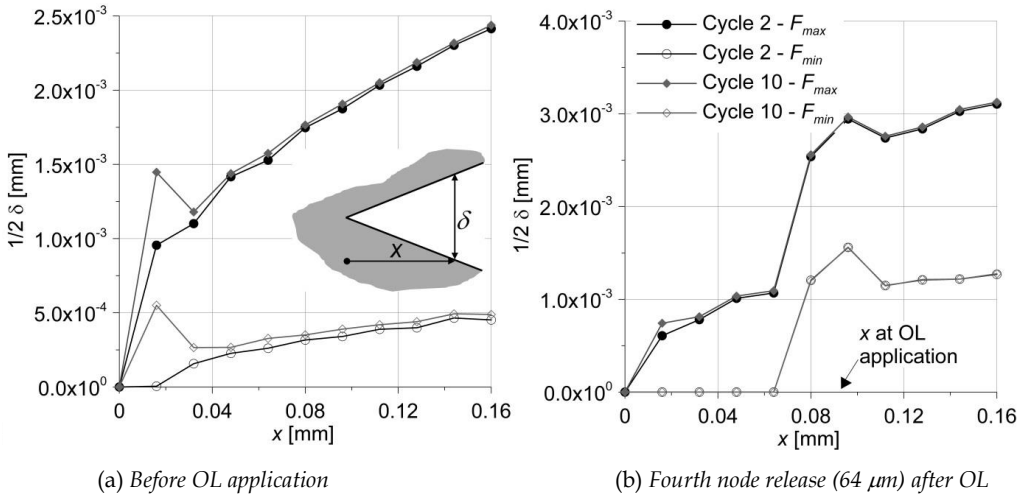


Figure 7: Crack flank position at minimum and maximum load in a steel SENB4 plane strain simulation with CA loading ( $R = 0.3$ ) and OL

of nodes in the wake, e.g. extrapolation with a second order polynomial of the positions of nodes 3 to 10, to the location at which the opening distance is zero. If this location is in the wake, it is assumed that the crack tip experiences closure. It appears that this method provides approximately the same crack opening stress as considering contact of the first node behind the crack tip in a simulation with node release each second cycle. The latter evaluation is easier, requires less computation time, and is therefore considered in the rest of this paper for plane strain cases.

Figure 7b provides the crack flank position for node releases after the application of an OL. The figure shows an abrupt change in crack flank position at the OL application, where contact is absent during the entire cycle in the wake before the point of OL whereas contact is experienced at minimum stress in the wake between the point of OL and the current crack tip position. For this situation a negligible movement of the first node behind the tip is observed during subsequent cycles and hence the evaluation of the crack opening stress is relatively straightforward after OL application.

## 4 Simulation results

### 4.1 Comparison with tests

The model results are compared with test results for validation purposes. Figure 8 provides the stress range effectivity ratio,  $U$ , as a function of the stress ratio,  $R$ . The curves represent equations from various literature sources that are based on test data for thin-walled sheet. The selected data are all in plane stress. The figure demonstrates two widely known observations:

- The stress range effectivity ratio increases – i.e.  $S_{\text{open}}$  decreases – for an increasing stress ratio.
- The stress range effectivity ratio at certain stress ratio is higher for steels than for aluminium alloys.

The dots in the figures represent the results from MT (plane stress) simulations with a mesh size of 16  $\mu\text{m}$ . The results of the simulations are in line with the test data. Note that the only difference between the steel and aluminium simulations are the parameters in the constitutive equations, Table 2. This indicates that the differences in crack opening stress between aluminium and steel are the result of differences in the stress-strain hysteresis.

The simulation of the aluminium alloy 6061-T4 at  $R = 0.1$  and  $S_{\text{max}} = 40$  MPa results in  $U =$

0.50 for a mesh of size  $8\ \mu\text{m}$ . As a comparison, Antunes et al. [33] simulated the same case using different software, a slightly different material model and a mesh size of  $16\ \mu\text{m}$  and they found  $U = 0.48$ .

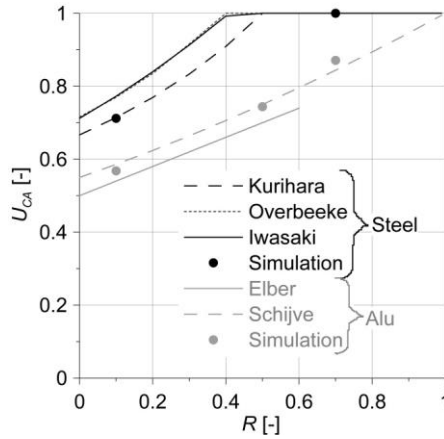


Figure 8: Ratio between effective and total stress intensity factor range as a function of stress ratio for plane stress resulting from tests (sources: [53]-[57]) and simulations of MT specimens (mesh size  $16\ \mu\text{m}$ )

In order to check the method for plane strain, the effect of OL-s on the opening stress of a SENB4 plane strain model is compared to a test carried out on a welded, stress relieved steel S355 specimens with the same dimensions as the model, Figure 4b, and a specimen thickness of 35 mm. The test is described in [47]. The specimen was loaded in CA with two OL-s with different maximum stress,  $S_{\max\text{ OL}}$ , with load data according to Table 3. The crack size,  $a$ , has been recorded as a function of the number of cycles,  $N$ , using crack gauges spaced 0.5 mm along the crack path. The cyclic stress-strain curve has not been determined for this case, however, the steel grade and chemical composition correspond with that of Table 2 and for this reason the hardening parameters of Table 2 are assumed applicable to the tested specimen.

Table 3: Load characteristics of the CA+OL test on a welded and stress relieved S355 steel SENB4 specimen

$S_{\min}$	$S_{\max}$ of CA	$S_{\max\text{ OL}}$ of 1st OL	$a$ at 1st OL	$S_{\max\text{ OL}}$ of 2nd OL	$a$ at 2nd OL
66 MPa	220 MPa	290 MPa	6 mm	372 MPa	8 mm

The effects of the two OL-s on the crack opening stress are evaluated using the FEM. Figure 9a presents the results of the model in terms of  $U$  as a function of the crack size,  $a$ . The figure indicates that  $U$  temporarily reduces after the application of the OL-s. The quantified effect on  $U$  is used to construct a crack growth curve by using the following procedure:

- a) The parametric relationship of [58] is used to determine  $\Delta K$  as a function of  $a$  for the SENB4 specimen:

$$\Delta K = Y(S_{\max} - S_{\min})\sqrt{\pi a} \quad (5)$$

where:

$$Y = \frac{0.923 + 0.199(1 - \sin \theta)^4}{\cos \theta} \sqrt{\frac{\tan \theta}{\theta}} \quad (6a)$$

$$\theta = \frac{\pi a}{2W} \quad (6b)$$

where  $W$  is the specimen height.

- b) The effective stress intensity factor range,  $\Delta K_{\text{eff}}$ , is determined by multiplying the total range with  $U$  obtained from the simulation (Figure 9a), Eq. (7). This provides a relationship between  $\Delta K_{\text{eff}}$  and  $a$ .

$$\Delta K_{\text{eff}} = U\Delta K \quad (7)$$

- c) The crack growth rate,  $da/dN$ , is determined from  $\Delta K_{\text{eff}}$  using Paris' equation:

$$\frac{da}{dN} = C\Delta K_{\text{eff}}^m \quad (8)$$

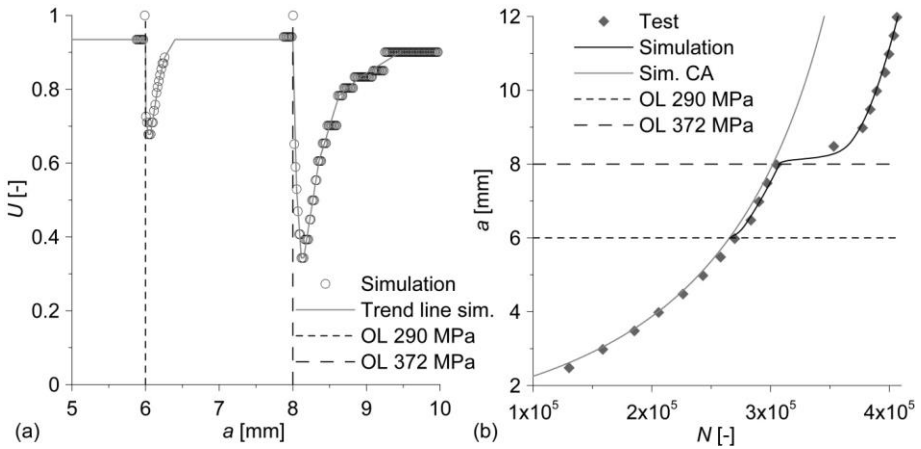
where  $m$  is a material constant taken as 3 and  $C$  is a material constant fitted to the CA part of the test. This results in  $C = 7.5 \cdot 10^{-14}$  (N, mm) for the steel SENB4 test.

- d) The number of cycles required for a crack extension from crack sizes  $a_i$  to  $a_f$  is determined by numerical integration of Eq. (8):

$$\Delta N_{\{a_i \text{ to } a_f\}} = \int_{a_i}^{a_f} \frac{da}{C\Delta K_{\text{eff}}^m} \quad (9)$$

The results of the test and the simulation thereof are plotted in Figure 9b. The simulation matches the experiment. Both the test (dots) and the simulation (curve) indicate that the

effect of the first OL on the crack growth is small but noticeable and that crack growth is substantially retarded after the second OL.



*Ratio between effective and total stress intensity factor range as a function of crack size resulting from the simulation*

*Crack size versus number of cycles resulting from test and simulation*

*Figure 9: Test and simulation of a steel SENB4 specimen loaded with CA and 2 OL*

The number of experiments and cases against which the model is checked here is too small to be able to speak of a fully validated model. Differences between actual and assumed constitutive parameters as well as differences between a 3D stress state and the assumed plane strain constraint influence the result. In addition, as explained before, the evaluation criteria are not straightforward and thus one should not rely only on the FEM results for quantifying crack growth retardation. But the comparison does show that the method is able to qualitatively grasp the correct trends, which is the purpose of this paper. It therefore provides a good basis for a comparison of different OL and UL scenarios. The following sections present such comparisons.

#### **4.2 Crack-closure of OL-s of different magnitude**

Unless specified otherwise, the simulations are carried out with a mesh of  $16 \mu\text{m}$ . Note that the results in terms of absolute values of  $U$  are depending on the mesh size and the selected mesh is coarser than the criterion of 2 to 3 elements in the reversed plastic zone. However, the intention of this section is not to provide exact values for  $U$ , but to provide

trends and to explain differences between materials and geometries instead. The mesh applied is suited for making such a comparison.

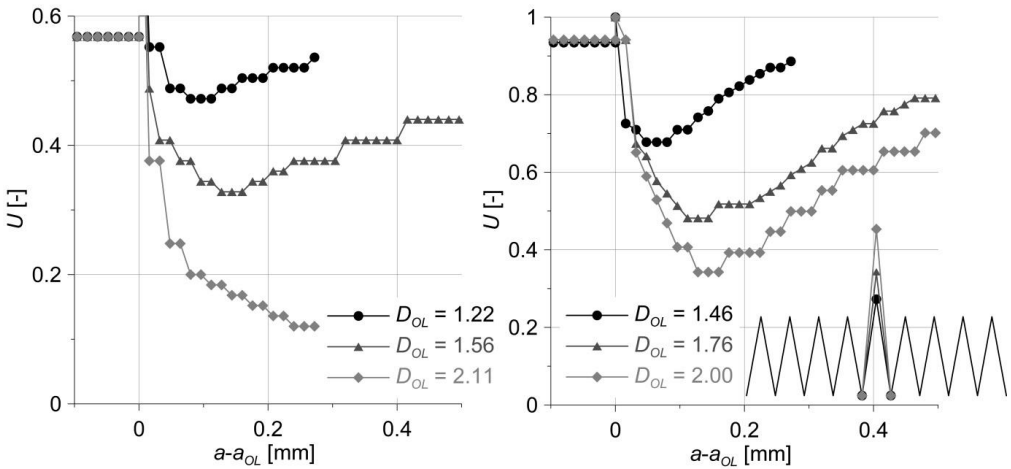
For presenting results, two indicators are used here to represent the OL magnitude relative to the CA stress ranges:

$$D_{OL} = \frac{S_{\max OL} - S_{\min}}{S_{\max} - S_{\min}} \quad (9)$$

$$A_{OL} = \frac{S_{\max OL}}{S_{\max}} \quad (10)$$

The first indicator -  $D_{OL}$  according to Eq. (9) - expresses the difference in stress range between OL and CA. The stress ratio  $R$  does not influence this indicator. On the other hand, the second indicator -  $A_{OL}$  according to Eq. (10) - expresses the difference in maximum stress between OL and CA. The minimum stress or stress range does not influence this indicator.

The change in  $U$  resulting from OLs of different magnitude is provided in Figure 10 for the case of an aluminium MT specimen loaded with  $R = 0.1$  and  $S_{\max} = 40$  MPa (Figure 10a) and a steel SENB4 specimen loaded with  $R = 0.3$  and  $S_{\max} = 220$  MPa (Figure 10b). The horizontal axis provides the crack size minus to the crack size at the overload. Hence the overload was applied at  $a - a_{OL} = 0$ .



(a) Specimen MT, 6016-T4, plane stress,  $R=0.1$  (b) Specimen SENB4, S355, plane strain,  $R=0.3$ )

Figure 10: Effects of overloads with different magnitude

Some observations from this figure are:

- The minimum value of  $U$  is obtained after a certain crack advancement following the application of the OL. This so-called delayed retardation is also observed in tests. The figure indicates that the larger  $D_{OL}$ , the larger is the delay.
- The crack growth required to cancel out the OL influence – i.e. the distance  $a - a_{OL}$  at which  $U$  approaches the preceding CA value – increases with increasing  $D_{OL}$ . Surprisingly, the results demonstrate that the rate at which  $U$  approaches the CA value after its minimum value is obtained, is independent of the overload ratio.
- For the largest OL ratio applied to the aluminium simulation ( $D_{OL} = 2.11$ ), the minimum value of  $U$  is so small that crack arrest is expected.

Figure 11 provides the deformations and the plastic strains perpendicular to the flank around the crack tip in an aluminium MT specimen loaded with  $R = 0.1$  and  $S_{max} = 40$  MPa at maximum load (left-hand graphs) and minimum load (right-hand graphs). The plastic zone created by the CA load in front of the crack tip – indicated with a red arrow – and at the wake of the crack resulting from the preceding loading and crack positions is presented in Figure 11a. The plastic zone commences from the initial crack which is indicated by a blue arrow. The stretched material in the plastic zone – well visible in the difference of the crack flank distance between the initial crack and the growing crack – is responsible for crack closure. The plastic zone changes abruptly at the application of an OL with  $D_{OL} = 1.56$ , Figure 11b. The increased stretching of the material resulting from the OL creates a local extension of the material at the crack flank. Figures 11c and d indicate that this local extension acts as a wedge and prevents closure of the flank further away from the tip. The wedge effect reduces as the crack grows further and the plastic zone increases gradually in size, Figure 11d, and reaches the size of that of a CA load after a large-enough crack extension (not displayed in the figure). The shape of the simulated flank shows a very good agreement with experimental observations presented elsewhere, such as a test on stainless steel in [59], see Figure 12.

Tests where the crack growth rate is accurately measured such as [3] and [45] indicate that the crack growth rate increases during the first few cycles directly after the application of an overload, followed by a gradual decrease up to the minimum value. This aspect is believed to be relevant especially in case of variable amplitude loading with various stress range magnitudes and a random sequence of stress ranges. Depending on the exact load

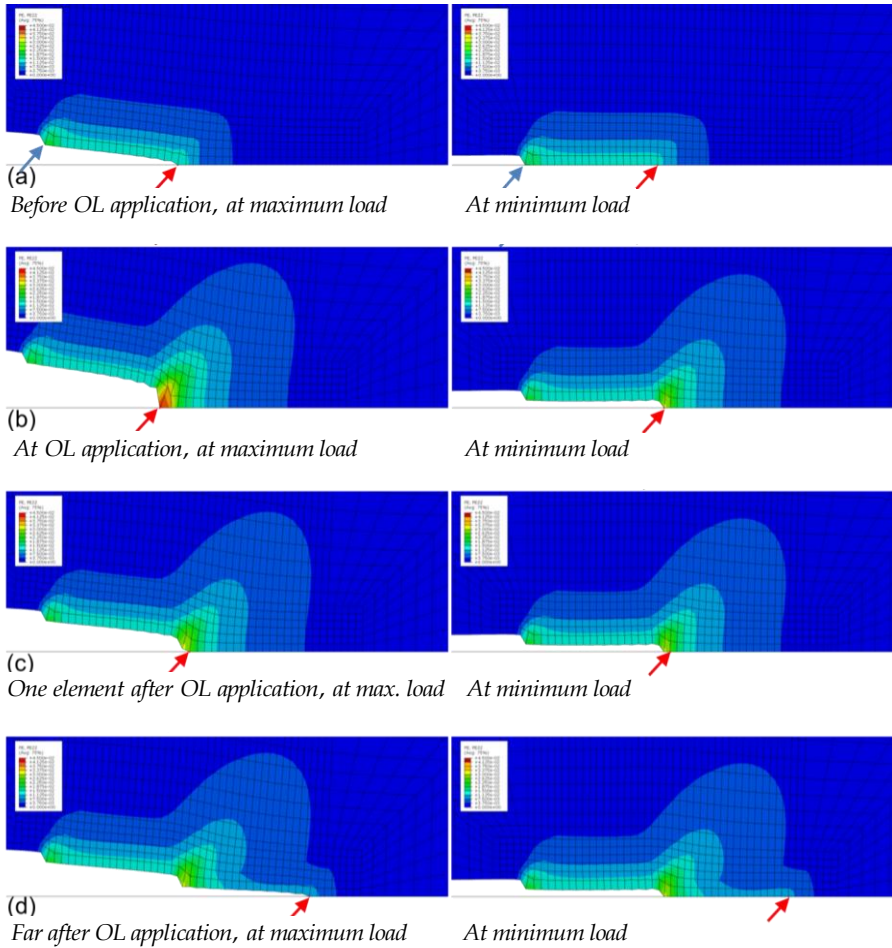


Figure 11: Evolution of the plastic strain perpendicular to crack before, during and after application of an overload (specimen MT, 6016-T4, plane stress,  $R = 0.1$ ,  $D_{OL} = 1.56$ )

Blue and red arrows indicate the initial and current crack tip position, respectively.



Figure 12: Crack flank before and after an overload, optical microscope image of 304L stainless steel. Image from [59]. Box left-hand side: initiation of the crack from a notch. Box right-hand side: crack flank developed after the overload.

sequence, a new stress peak may be applied before the minimum crack growth rate of the previous peak is reached and the accelerated crack growth may compensate or even dominate over the retardation effect. The accelerated crack growth during these first cycles following an overload can be well explained by considering the deformation of Figure 11b. The figure shows that the crack flanks are not in contact at minimum stress directly following the OL. This implies that the full stress cycle is effective in the first cycles following an OL. This is also demonstrated in the evaluation of  $U$  in a CA simulation with an OL, where a CA stress cycle is applied after the OL and before an additional node is released, i.e. without crack extension between the OL and the subsequent first CA cycle, Figure 13. The figure indicates that  $U$  increases to unity during that CA stress cycle. A similar analysis with crack closure after an OL is reported [45] but the acceleration effect was not observed in that simulation. This is expected to be caused by the fact that nodes were released at maximum load in [45], whereas they were released at minimum load in the current paper. This example demonstrates that the choices in parameters have consequences on the result and that the FEM is able to give a qualitative view of the processes only. In addition, crack tip blunting – which is especially large at the OL as observed in Figure 11 – may cause that a crack needs to initiate directly after the OL and this may also contribute to crack growth retardation. This cannot be simulated with the type of model used. However, the trend is clear and agrees with the qualitative

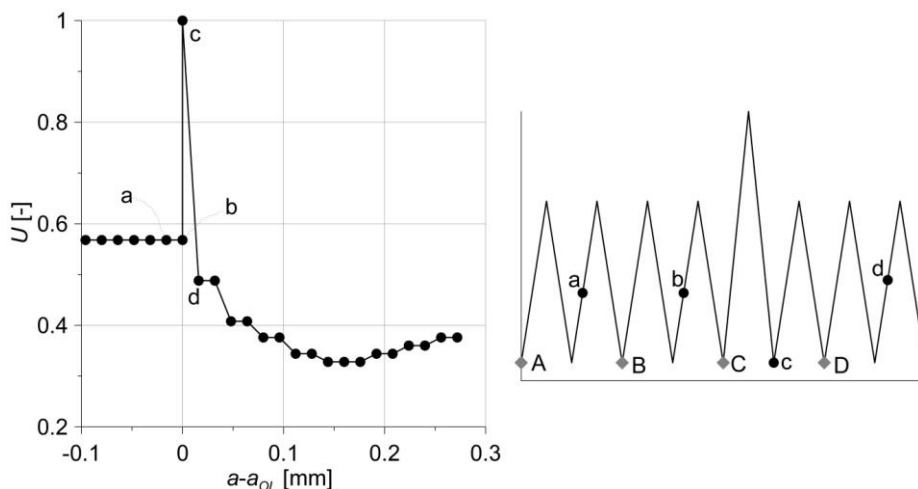


Figure 13: Effect of an OL ( $D_{OL} = 1.56$ ) where a CA cycle is applied after the OL without crack extension, resulting in a peak value for  $U$ . Node releases at A, B, C and D, crack opening at a, b, c and d

experimental observations of crack growth acceleration during the first cycles following overload followed by (delayed) retardation.

An important indicator for the amount of crack growth retardation is the ratio between the minimum effectivity ratio after an overload and the effectivity ratio at constant amplitude loading,  $U_{\min\text{OL}} / U_{\text{CA}}$ . Figure 14 gives this ratio as a function of the overload ratio resulting from simulations with different geometries, constraints, and materials. Note that both  $U_{\text{CA}}$  and  $U_{\min\text{OL}}$  vary substantially for the cases considered. Despite these differences, the figure indicates that the relationship between  $D_{\text{OL}}$  and the ratio  $U_{\min\text{OL}} / U_{\text{CA}}$  is fairly constant for all cases. However, note that:

- This study is set-up to provide understanding and explain trends in  $U$ , not to provide exact values for  $U$ . The message of the figure is that the ratio  $U_{\min\text{OL}} / U_{\text{CA}}$  decreases with increasing  $D_{\text{OL}}$ .
- The ratio  $U_{\min\text{OL}} / U_{\text{CA}}$  is not the only indicator for the crack growth retardation magnitude, as is demonstrated in the following sections.

Some outliers in the figure origin from the presentation method. As an example, the three encircled cases in Figure 14 are for relatively high stress ratios and relatively low stress ranges. The figure indicates that these cases give a higher ratio  $U_{\min\text{OL}} / U_{\text{CA}}$  (hence less retardation) as compared to the other cases if assessed with  $D_{\text{OL}}$ , but the opposite is true if assessed using  $A_{\text{OL}}$ . This indicates that nor  $D_{\text{OL}}$ , nor  $A_{\text{OL}}$  is a good evaluation criterion for the amount of retardation, and that both the stress range and the  $R$ -ratio influence the amount of retardation.

#### 4.3 Crack-closure for different materials and geometries

The influence of material on the ratio  $U_{\min\text{OL}} / U_{\text{CA}}$  is indicated in Figure 15a, where results are presented of MT specimens in plane stress of different materials with  $D_{\text{OL}} = 1.55$  and  $R = 0.1$ . The figure indicates that DIN-CK45 provides larger ratios of  $U_{\min\text{OL}} / U_{\text{CA}}$  than the other two materials. However, although  $U_{\min\text{OL}} / U_{\text{CA}}$  for S355 is close to that of the aluminium alloy, the plot of  $U$  as a function of crack length gives a different view, Figure 15b. This figure considers the analysis of two different materials with further equal geometry and load conditions ( $S_{\max} / S_y = 0.323$ ,  $R = 0.1$ ,  $D_{\text{OL}} = 1.56$ ). The figure shows that the delayed retardation period of the aluminium alloy is significantly shorter than that of the steel grade. This was also observed in experiments in [3]. The figure shows that the

crack experiences less crack closure for a crack advancement of 0.08 mm after the OL application. In this crack advancement period, the crack growth rate accelerates before it retards.

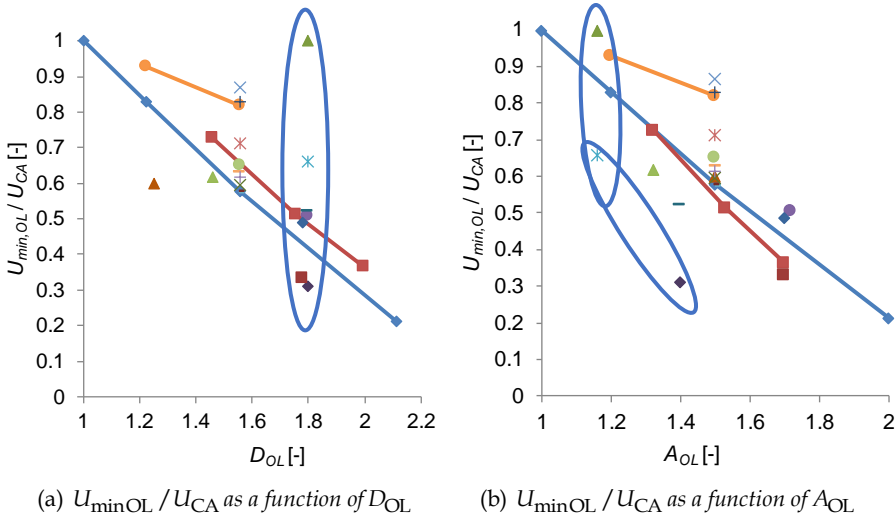


Figure 14: Relationship between overload ratio and stress range effectivity ratios for different geometries and load conditions

- AA6016-T4, MT, pl.σ, ΔS = 36, R = 0.1
- ◆ AA6016-T4, MT, pl.σ, ΔS = 36, R = 0.5
- AA6016-T4, MT, pl.σ, ΔS = 24, R = 0.1
- AA6016-T4, MT, pl.σ, ΔS = 54, R = 0.1
- ▲ AA6016-T4, MT, pl.σ, ΔS = 20, R = -1
- + DIN CK45, MT, pl.σ, ΔS = 72, R = 0.1
- DIN CK45, MT, pl.ε, ΔS = 72, R = 0.1
- × DIN CK45, MT, pl.σ, ΔS = 144, R = 0.1
- × DIN CK45, MT, pl.ε, ΔS = 144, R = 0.1
- S355, MT, pl.ε, ΔS = 72, R = 0.1
- × S355, MT, pl.σ, ΔS = 72, R = 0.1
- S355, MT, pl.ε, ΔS = 135, R = 0.1
- + S355, MT, pl.σ, ΔS = 135, R = 0.1
- ▲ S355, SENB4-a, pl.σ, ΔS = 153.8, R = 0.3
- S355, SENB4-a, pl.ε, ΔS = 153.8, R = 0.3
- S355, SENB4-a, pl.ε, ΔS = 153.8, R = 0.1
- S355, SENB4-a, pl.ε, ΔS = 153.8, R = 0.5
- × S355, SENB4-a, pl.ε, ΔS = 60, R = 0.8
- S355, SENB4-b, pl.σ, ΔS = 216, R = 0.1
- ◆ S355, SENB4-b, pl.ε, ΔS = 216, R = 0.1
- ▲ S355, SENB4-b, pl.ε, ΔS = 30, R = 0.8

The difference in behavior between the materials can be attributed to the cyclic stress-strain relationship, because the only differences between the simulations are the values of the material coefficients. To better understand this influence, Figure 16 provides the cyclic stress-strain hysteresis in the Gauss point (GP) closest to the crack tip at which the OL is applied. The more pronounced Bauschinger effect for the steel case results in more plasticity in compression. In combination with smaller isotropic hardening, this results in a larger reversed plastic zone for steel. Another consequence is that the maximum strain at

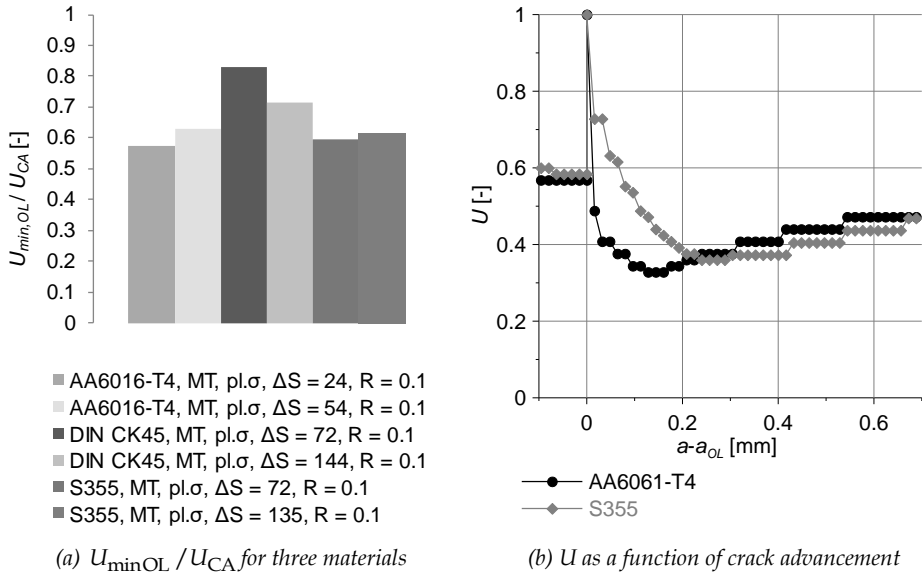


Figure 15: Comparison of retardation for three materials at  $D_{OL} = 1.56$

the OL is more than two times larger than that of the aluminium case. Similarly, when the crack tip position has passed and the GP is in the crack wake, the steel GP experiences reversed plasticity whereas the aluminium GP experiences an elastic stress only. To summarise, more material participates in the reversed plastic zone in the steel case as

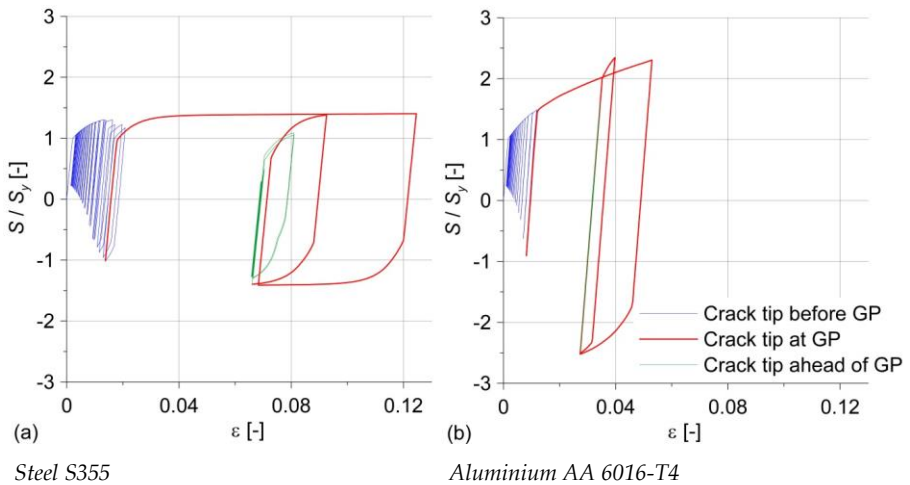


Figure 16: Stress-strain hysteresis at the GP closest to the OL application for different materials (Specimen MT, plane stress,  $R = 0.1$ ,  $D_{OL} = 1.56$ )

compared to the aluminium case, both in front of the crack tip and in the wake. This will have a subduing effect on crack closure at the overload and it is believed to cause the larger delayed retardation period in the steel case.

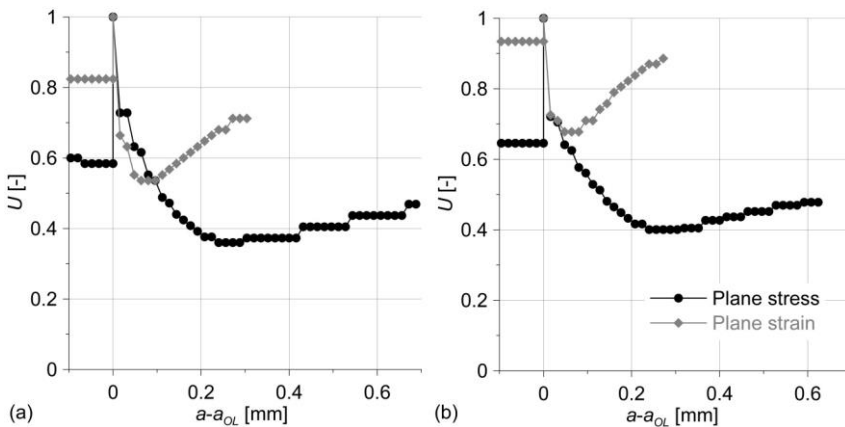
Figure 17 provides an investigation into the constraint effect in combination with an OL.

The figure indicates that:

- The crack opening stress for plane stress at CA loading (for  $a < a_{OL}$ ) is significantly larger than for plane strain.
- The minimum value of  $U$  for plane stress is obtained further away from the OL application than for plane strain, i.e. the delay of crack growth retardation is larger for plane stress than for plane strain.

The retardation effect lasts longer in plane stress as compared to plane strain.

These observations are consequences of the larger plastic zone in plane stress as compared to plane strain. Figure 18 provides the cyclic stress-strain hysteresis of the steel MT plane strain case at a GP closest to the crack tip at which the OL is applied. The figure can be compared with the plane stress simulation of Figure 15a. The larger constraint for plane strain results in a larger tangent stiffness in the plastic region and consequently a smaller maximum strain at application of the OL (red curve). In case of plane stress, negative strains are experienced during a part of the CA stress cycle which is not the case for plane strain (blue curve).



Specimen MT, S355, R=0.1, DOL=1.56

Specimen SENB4, S355, R=0.3, DOL=1.46

Figure 17: Effects of overloads at different constraints

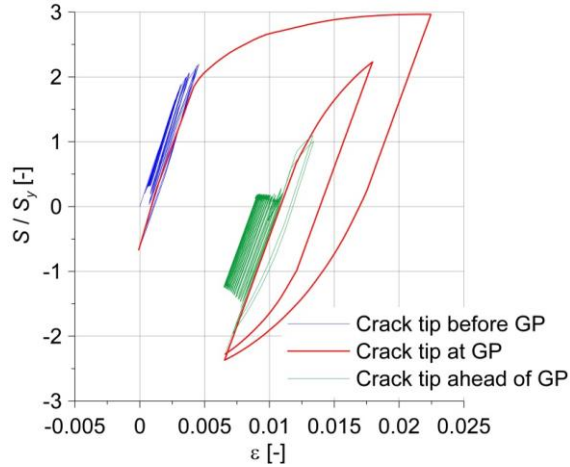


Figure 18: Effects of an overload in a plane strain state (Specimen MT, S355,  $R = 0.1$ ,  $D_{OL} = 1.56$ )

As indicated in the introduction of this paper, there exists debate on the possibility of crack closure in plane strain because the extra material required for plastic stretching in the wake of the crack cannot originate from the thickness direction. The simulations presented in this paper, however, indicate crack closure in plane strain especially after an OL. A possible explanation is provided in [24]: the extra material originates from further down the crack flank, i.e. the material is transported from the flank towards the crack tip. This is also observed in the simulations carried out in the current research and becomes apparent when considering the stress-strain hysteresis when the GP is in the wake (green curve in Figure 18). This curve indicates that the strain decreases in each cycle despite the relatively low stress values. This apparent shrinkage of material in the wake is caused by the earlier mentioned material transport to the tip and is not observed in any of the plane stress simulations.

Apart from the constraint in thickness direction, Figure 17 demonstrates that the specimen type is also important for crack closure. The values of  $U_{CA}$  are larger for the SENB4 specimens than for the MT specimens. This difference is larger for plane strain than for plane stress. A possible explanation for this difference is the fact that the crack in the SENB4 specimens opens more easily due to the absence of mid plane constraints. Notably, the ratios  $U_{min} / U_{CA}$  are approximately the same for the two types of specimen.

#### 4.4 Effects of underloads and overload-underload combinations

Tests have indicated that UL-s may cause a slight acceleration of crack growth, [7]-[9]. Some simulations have been carried out with single UL-s and with combinations of OL-s and UL-s. The underload ratio,  $D_{UL}$ , is defined as:

$$D_{UL} = \frac{S_{max} - S_{minUL}}{S_{max} - S_{min}} \quad (11)$$

Figure 19 provides the results of a simulation with an UL. The value of  $U$  increases slightly following the application of an UL, Figure 19a, but the effect is much smaller to that of an OL with similar magnitude. The UL presses the crack flanks firmly together and creates a locally smaller zone with high plastic strains, Figure 19b. The material is thus stretched less due to the UL and this explains the observed increase in crack opening stress. The lower acceleration at an UL as compared to retardation at an OL of similar magnitude is attributed to the fact that the entire flank is participating in the load transfer in case of an UL, and not just the crack tip as in case of the OL.

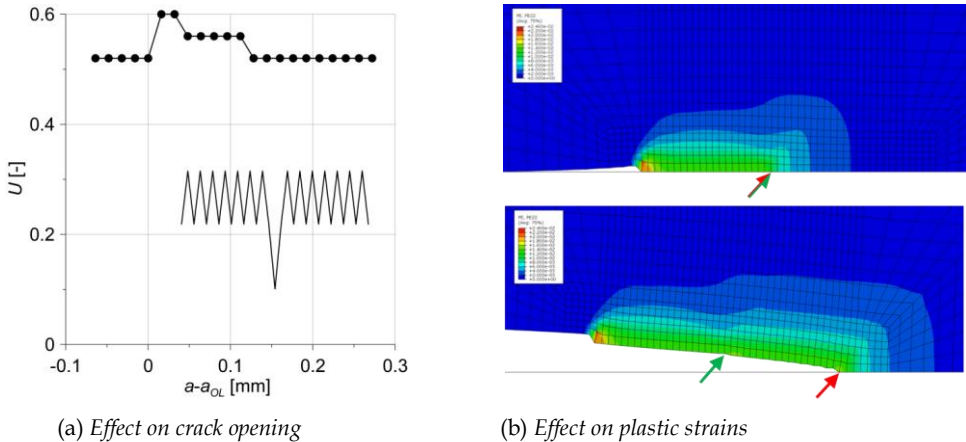


Figure 19: Simulation of a specimen subjected to an UL

MT, 6016-T4, plane stress,  $R = 0.1$ ,  $D_{UL} = 2.22$

Red and green arrows indicate the current and OL crack tip position, respectively.

Tests have demonstrated that the combined effects of OL-s and UL-s on the crack growth rate in a variable amplitude spectrum is different from the arithmetic sum of retardation and acceleration effects of individual OL-s and UL-s [10]-[12]. Several studies have shown

that the retardation effect of OL is almost cancelled if followed by an UL. However, a recent experimental study has concluded that the OL effect is still dominant, [60]. To investigate this case, Figure 20 provides the development of the stress range effectivity ratio resulting from a single OL, a single UL, an OL followed by an UL (OL-UL) and an UL followed by an OL (UL-OL). Except for the single UL, all cases create a decrease of  $U$  after some crack advancement. The analysis of an OL preceded by an UL (UL-OL) indicates that the influence of the UL is completely cancelled out and the effective stress range is equal to that of a single OL. Thus, for this case, the UL has no effect on crack retardation. The OL followed by UL (OL-UL) provides a smaller reduction of  $U$  as compared to the case of a single OL. The bulging at the crack flank created by the OL is flattened by the succeeding UL. Thus, in this case, the UL partially cancels the effect of the OL. It is interesting to observe that crack acceleration is larger and lasts longer for the OL-UL case as compared to the single UL case. This is expected to have a large influence in case of VA loading with stress peaks and valleys of different magnitudes in random sequence. It may explain the observed apparent absence of retardation of even acceleration in tests with such VA loads reported in [12] and [47].

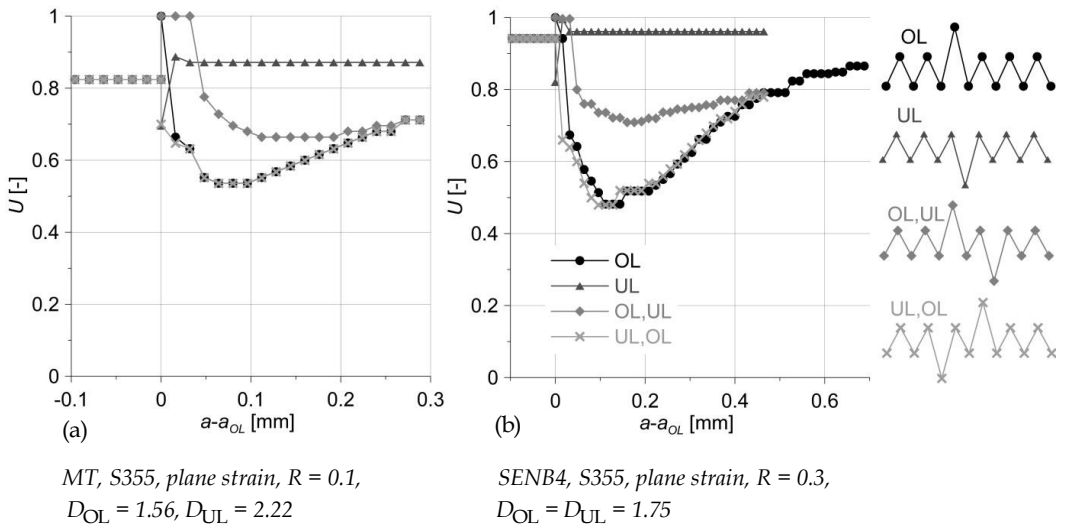


Figure 20: Combinations of overloads and underloads

#### 4.5 The influence of residual stress

Residual stress, e.g. caused by shrinkage during cooling of a welded specimen, may influence the crack closure levels and effects of retardation. The effect of adding residual stress may be different from that of increasing the external load because:

- Residual stresses are resulting from imposed deformations and not imposed loads. As the crack advances, the constraint effect is reduced and residual stresses may reduce.
- For sufficiently high values of residual stresses in combination with the external loads applied, strain values may exceed those related to the yield or 0.2 % proof stress.

Additional simulations of PICC using the FEM have been run in order to determine the influence of residual stress levels. The residual stress is introduced by adding the coefficient of linear thermal expansion to the constitutive equations and by adding a temperature profile that was selected in such a case as to result into realistic residual stresses. This was done before the external cyclic loads were applied to the model. An example of the residual stress pattern is indicated in Figure 21. The residual stress value reported hereafter is the value experienced at the crack tip.

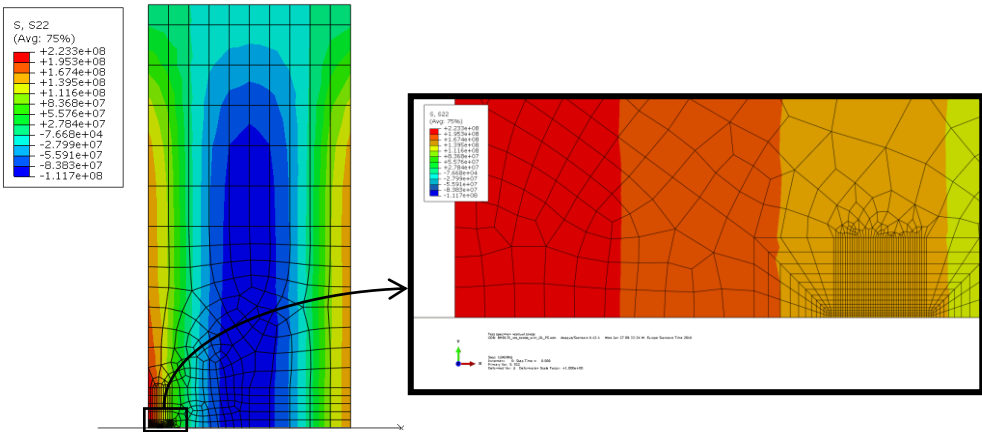


Figure 21: Example of a residual stress field applied in the FEM

Figure 22 provides the results in terms of  $U_{\min OL} / U_{CA}$  for cases without residual stresses (in grey) and with residual stresses (in red). Indicator  $A_{OL}$  is in this case defined including residual stresses, hence:

$$A_{OL} = \frac{S_{\max OL} + S_{\text{res}}}{S_{\max} + S_{\text{res}}} \quad (12)$$

The figure indicates that the trend as experienced for the cases without residual stresses – larger overloads result in lower values of  $U_{\min OL}$  – is no longer present in case of residual stresses. In general, adding residual stresses reduces the  $U_{\min OL}$  level especially at large

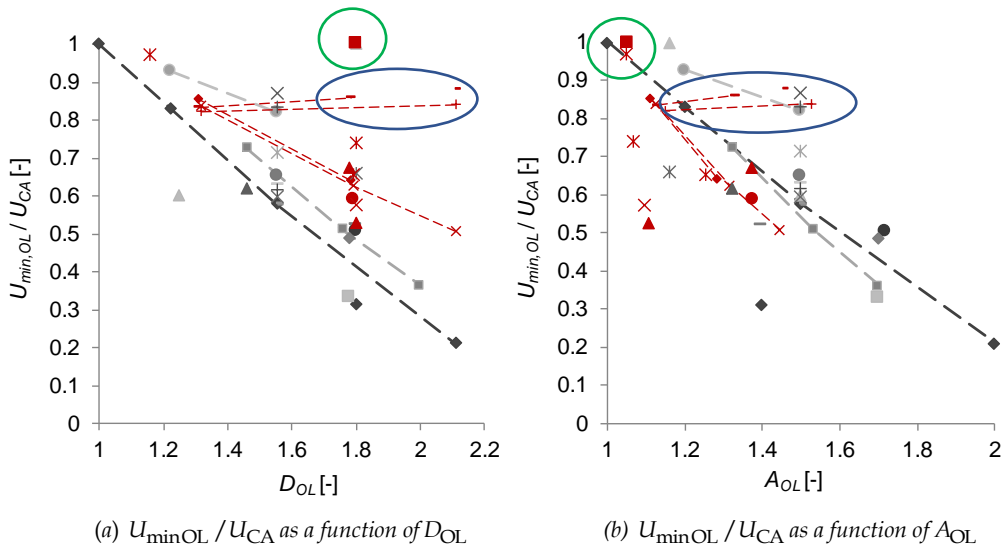


Figure 22: Relationship between overload ratio and stress range effectivity ratios for different geometries and load conditions

- ◆— AA6016-T4, MT, pl.σ, ΔS = 36, R = 0.1
- ◆ AA6016-T4, MT, pl.σ, ΔS = 36, R = 0.5
- AA6016-T4, MT, pl.σ, ΔS = 24, R = 0.1
- AA6016-T4, MT, pl.σ, ΔS = 54, R = 0.1
- ▲ AA6016-T4, MT, pl.σ, ΔS = 20, R = -1
- + DIN CK45, MT, pl.σ, ΔS = 72, R = 0.1
- DIN CK45, MT, pl.ε, ΔS = 72, R = 0.1
- × DIN CK45, MT, pl.σ, ΔS = 144, R = 0.1
- × DIN CK45, MT, pl.ε, ΔS = 144, R = 0.1
- S355, MT, pl.ε, ΔS = 72, R = 0.1
- × S355, MT, pl.σ, ΔS = 72, R = 0.1
- S355, MT, pl.ε, ΔS = 135, R = 0.1
- + S355, MT, pl.σ, ΔS = 135, R = 0.1
- ▲ S355, SENB4-a, pl.σ, ΔS = 153.8, R = 0.3
- S355, SENB4-a, pl.ε, ΔS = 153.8, R = 0.3
- S355, SENB4-a, pl.ε, ΔS = 153.8, R = 0.1
- S355, SENB4-a, pl.ε, ΔS = 153.8, R = 0.5
- × S355, SENB4-a, pl.ε, ΔS = 60, R = 0.8
- S355, SENB4-b, pl.σ, ΔS = 216, R = 0.1
- ◆ S355, SENB4-b, pl.ε, ΔS = 216, R = 0.1
- ▲ S355, SENB4-b, pl.ε, ΔS = 30, R = 0.8
- ▲ S355, SENB4-b, pl.ε, ΔS = 216, Sres = 210, R = 0.1, Rres = 0.5
- ×- S355, SENB4-b, pl.ε, ΔS = 151.2, Sres = 210, R = 0.1, Rres = 0.6
- × S355, SENB4-b, pl.ε, ΔS = 151.2, Sres = 300, R = 0.1, Rres = 0.7
- S355, SENB4-b, pl.ε, ΔS = 151.2, Sres = 150, R = 0.1, Rres = 0.5
- + S355, SENB4-b, pl.σ, ΔS = 151.2, Sres = 150, R = 0.1, Rres = 0.5
- S355, SENB4-b, pl.σ, ΔS = 151.2, Sres = 200, R = 0.1, Rres = 0.6
- - S355, SENB4-b, pl.σ, ΔS = 156, Sres = 150, R = 0.3, Rres = 0.6
- ◆- S355, SENB4-b, pl.ε, ΔS = 156, Sres = 210, R = 0.3, Rres = 0.6
- S355, SENB4-b, pl.ε, ΔS = 30, Sres = 300, R = 0.8, Rres = 0.9
- ▲ S355, SENB4-b, pl.ε, ΔS = 60, Sres = 150, R = 0.8, Rres = 0.9
- × S355, SENB4-b, pl.σ, ΔS = 60, Sres = 200, R = 0.8, Rres = 0.9
- × S355, SENB4-b, pl.σ, ΔS = 30, Sres = 200, R = 0.8, Rres = 0.9

values of  $D_{OL}$ . The figure suggests for two cases that  $U_{\min,OL}$  even increases at increasing  $D_{OL}$ . However, this is believed to be a result of the discretization of the FEM results; in reality  $U_{\min,OL}$  is expected to remain constant in these cases.

The residual stress cases that deviate significantly from the trend line of the cases without residual stresses – encircled in blue in the graph – are plane stress cases with relatively

large values of residual stress plus overload. In these cases, global plasticity may have taken place and this may have an influence on the results. Due to global plasticity, the case with large residual stress may be different from the case of high external load ratio and without residual stresses. Hence, such conditions must be treated with care if one accounts for retardation effects. It should be noted that the duration of retardation in terms of crack advancement at which  $U$  again reaches  $U_{CA}$  is not altered, hence retardation effects remain present.

A final case to be considered is the dot encircled in green in Figure 22. This case, showing no or only small retardation, has a small stress range at large stress ratio and large residual stress. In such a case, with high relevancy for practice, retardation is not to be expected. The same case has been run without residual stress and the same result was found: significant retardation is not observed (the dots are overlapping in Figure 22, see Figure 14 for this individual case).

## 5 Discussion on VA loading and the near-threshold regime

A vast number of tests with a single OL in a further CA load regime have clearly demonstrated the presence of crack growth retardation due to the OL. On the other hand, VA tests with a mixed, ergodic stress range variation and sequence show ambiguous results. Schijve [61] tested load sequences ordered in blocks from minimum to maximum stress range or vice versa on aluminium specimens and demonstrated that the load sequence effect in blocks with a large number of cycles per block (400000) was significantly larger as compared to that of a random load sequence or an ordered sequence with a small number of cycles per block (40). Maljaars et al. [47] carried out VA fatigue tests on thick C-Mn steel welded specimens in as welded and in stress relieved condition and they showed that the average crack growth rate in case of random loading was approximately two times higher as compared to CA loading, i.e. the net load sequence effect was crack growth *acceleration*. In case of ordered in blocks from minimum to maximum stress range and back, the crack growth rate was approximately three times lower as compared to the CA loading, i.e. the net load sequence effect was crack growth retardation. Zhang and Maddox [12] tested welded steel specimens with random loading in which the maximum stress was kept constant (sequence A), or the minimum stress (sequence C), or both maximum and minimum stresses were variable (sequence B). The tests with sequence C resulted in significant longer lives – i.e. retardation – but the tests with sequence A resulted in shorter

life – i.e. acceleration – as compared to the CA loading tests. The tests with sequence B had a life comparable to that of the CA loading.

Considering the results of the simulations, the following possible causes are provided for these ambiguous results in case of VA load:

- Overloads and underloads continuously follow up in a VA load sequence. This study has shown that if an OL is followed by an UL of similar magnitude, the effect of the OL is significantly reduced or even cancelled out.
- After the application of an OL, crack growth initially accelerates before it retards. This was observed in both experiments and numerical simulations. The zone (or period) over which acceleration takes place is larger for steel than for aluminium, related to differences in cyclic hardening of these materials. The net retardation effect comes to full development only if the crack is able to advance over a certain distance without additional events. In realistic loading conditions, however, new OL (or UL) events are to be expected before the crack has advanced to this distance, see Figure 23.

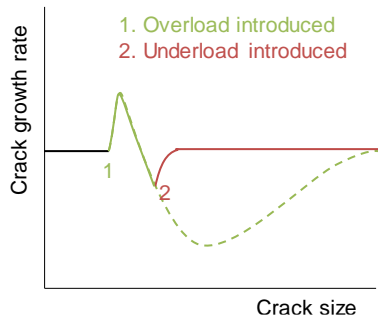


Figure 23: Crack growth rate at an OL and at an OL followed by an UL

The threshold stress intensity factor,  $\Delta K_{th}$ , describes the range of the stress intensity factor at which crack growth does not occur. Many experts believe that PICC is especially relevant in the near-threshold regime, [16]. They indicate that the sensitivity of  $\Delta K_{th}$  on the stress ratio  $R$  is due to PICC: at a certain level of plasticity in the wake, the crack opening stress is larger than the maximum stress applied in a small cycle and hence crack growth does not take place. The dependency on stress ratio is much larger for the threshold regime than for the part of the crack growth curve with constant rate, Figure 24.

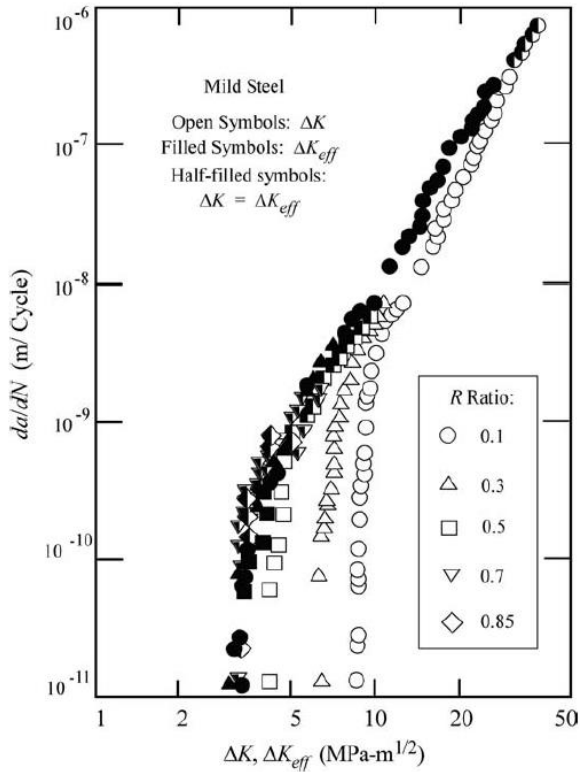


Figure 24: Fatigue crack growth data near the threshold for mild steel at various stress ratios [62], (reprinted from [16])

Following this explanation of stress-ratio dependency of the crack growth threshold,  $\Delta K_{th}$  is expected to be altered by over- and underloads. In the area of retardation following an  $OL$ , closure levels are larger than in  $CA$  loading and this increases the threshold value. For practical applications this may have a significant influence, as there are often many cycles in the near threshold range. This would imply that these cycles do no longer contribute to crack growth.

On the other hand, whereas single  $UL$  have a small accelerating effect on the crack growth in a further  $CA$  load regime, a reduction of the threshold may result. This expectation is based on the observation of the simulations in this section that the wake is flattened due to the  $UL$ . This aspect may explain the lower fatigue life than expected [12] and significant contribution of small stress cycles [63] in a  $VA$  load history where the maximum stress is kept constant and the minimum stress is varied.

The expected effects on the near threshold regime of OL-s and UL-s explained in this section only hold in case of OL-s and UL-s with large magnitude. The simulation result encircled in green in Figure 22 indicates that a spectrum with stress ranges that are all of small to medium magnitude do not result in a change in crack closure level. This is strictly shown for an OL only but there is no reason to believe that an UL of small magnitude will have a significant influence on plasticity levels.

## 6 Conclusions

The crack growth retardation and acceleration effects resulting from (a combination of) an OL and an UL have been determined with the FEM. The model consists of conventional elements with a dense mesh at the crack tip and a material model allowing for cyclic isotropic and kinematic hardening. Crack growth was not explicitly modeled. Instead, nodes were released and the stress at which the crack opened was evaluated. Different constraints (plane stress and plane strain), specimen geometries (MT, SENB4) and materials (steel, aluminium) were considered. A number of choices have to be made related to evaluation criteria which makes that the quantitative effect of crack closure resulting from the method should not be relied upon without experimental support. However, the method helps explaining the physical phenomena responsible for crack closure and retardation.

The initial acceleration observed in experiments during the first cycles directly after the application of an OL is attributed to the large zone with stretched material of the OL which causes the entire crack to be open during the full cycle. The gradual decrease of the crack growth rate – so-called delayed retardation – and subsequent gradual increase of the rate up to the attainment of the CA rate which have been observed in many experiments can be explained by considering the crack flank profile after the OL in combination with the plastic zone in front of the crack. The higher effective stress range during CA loading and longer delayed retardation period of steel in comparison to aluminium are due to different cyclic hardening. Crack closure in plane strain following an OL is made possible by material transport from the wake to the tip of the crack. It is further observed that retardation following an OL is still present in cases where the CA loadcase results in a fully effective stress range.

An UL causes crack growth acceleration. However, the acceleration is smaller as compared to retardation following an OL of similar magnitude because of the larger crack flank area involved in transferring the UL. The combined effect of an OL followed by an UL of similar magnitude provides crack growth acceleration followed by retardation. Contrarily, the combined effect of an UL followed by an OL is equal to that of a single OL, i.e. there is no effect of the UL in this case.

Experiments demonstrate ambiguous results with respect to crack growth rates in case of VA loading with fully mixed (ergodic) sequence of cycles. This is attributed to continuous follow-up of OL and UL, where there is not always sufficient distance between OL's for full development of the plastic wake.

#### *Acknowledgements*

This research is sponsored by the framework TKI Wind op Zee. The authors would like to thank the co-sponsors and partners Arcelor Mittal, Keppel Verolme, VGB and Noordzeewind.

## References

- [1] Shin CS, Fleck NA. Overload retardation in a structural steel. *Fatigue Fract Engng Mater Struct* 1987;9:379-93.
- [2] Tanaka K, Matsuoka S, Schmidt V, Kuna M. Influence of specimen geometry on delayed retardation phenomena of fatigue crack growth in HT80 steel and AA5083 Aluminium Alloy, In: Francois D, editor. *Proc 5th Int Conf Fract 4*, Cannes: Pergamon press; 1981, p. 1789-98.
- [3] Wang C, Wang X, Ding Z, Xu Y, Gao Z. Experimental investigation and numerical prediction of fatigue crack growth of 2024-T4 aluminum alloy. *Int J Fatigue* 2015;78:11-21.
- [4] Werner K. The influence of strain conditions in steel samples on the fatigue crack growth and delay after overload. *Sol St Phen* 2015;224:151-6.
- [5] Matsuoka S, Tanaka K. The influence of sheet thickness on delayed retardation phenomena in fatigue crack growth in HT80 steel and A5083 aluminium alloy. *Eng Fract Mech* 1980;13:293-306.
- [6] Shercliff HR, Fleck NA. Effect of specimen geometry on fatigue crack growth in plane strain-II. Overload response. *Fatigue Fract Engng Mater Struct* 1990;3:297-310.
- [7] Zheng X, Cui H, Engler-Pinto CC, Su X, Wen H. Numerical modeling of fatigue crack propagation based on the theory of critical distances: Effects of overloads and underloads. *Eng Fract Mech* 2014;128:91-102.
- [8] Benz C, Sander M. Experiments and interpretations of some load interaction phenomena in fatigue crack growth related to compressive loading. *Adv Mat Res* 2014;891:1353-9.
- [9] Doré MJ, Maddox SJ. Accelerated fatigue crack growth in 6082 T651 aluminium alloy subjected to periodic underloads. *Procedia Engineering* 2013;66:313-22.
- [10] Qian Y, Cui W-C. An overview on experimental investigation on variable amplitude fatigue crack growth rule. *J Ship Mech* 2010;14:556-65.
- [11] Romeiro F, De Freitas M, Da Fonte M. Interaction effects due to overloads and underloads on fatigue crack growth. *Key Eng Mat* 2007;348-349:333-6.
- [12] Zhang YH, Maddox SJ. Investigation of fatigue damage to welded joints under variable amplitude loading spectra, *Int J Fatigue* 2009;31:138-52.
- [13] Sadananda K, Vasudevan AK. Multiple mechanisms controlling fatigue crack growth. *Fatigue Fract Eng Mater Struct* 2003;26:835-45.

- [14] Toribio J, Kharin V. Simulations of fatigue crack growth by blunting-re-sharpening: Plasticity induced crack closure vs. alternative controlling variables. *Int J Fatigue* 2013;50:72-82.
- [15] Alderliesten RC. How proper similitude can improve our understanding of crack closure and plasticity in fatigue. *Int J Fatigue* 2016;82:263-73.
- [16] Anderson TL. *Fracture Mechanics: Fundamentals and applications*. 3rd ed. Boca Raton: Taylor and Francis; 2005.
- [17] Ewalds HL, Furnée RT. Crack closure measurements along the crack front in center cracked specimens. *Int J Fract* 1978;14:R53-5.
- [18] Gonzalez-Herrera A, Zapatero J. Tri-dimensional numerical modelling of plasticity induced fatigue crack closure. *Eng Fract Mech* 75;2008:4513-28.
- [19] Matos PFP, Nowell D. The influence of the Poisson's ratio and corner point singularities in three-dimensional plasticity-induced fatigue crack closure: a numerical study. *Int J Fatigue* 2008;30:1930-43.
- [20] Vor K, Gardin C, Sarrazin-Baudoux C, Petit J. Wake length and loading history effects on crack closure of through-thickness long and short cracks in 304L: Part II - 3D numerical simulation. *Eng Fract Mech* 2013;99:306-23.
- [21] Solanki K, Daniewicz SR, Newman Jr JC. Finite element modelling of plasticity-induced crack closure with emphasis on geometry and mesh refinement effects. *Eng Fract Mech* 2003;70:1475-89.
- [22] Sehitoglu H, Sun W. Modelling of plane strain fatigue crack closure. *ASME J Eng Mat Technol* 1991;113:31-40.
- [23] Lugo M, Daniewicz SR. The influence of T-stress on plasticity induced crack closure under plane strain conditions. *Int J Fatigue* 2011;33:176-85.
- [24] Antunes FV, Chegini AG, Branco R, Camas D. A numerical study of plasticity induced crack closure under plane strain conditions. *Int J Fatigue* 2015;71:75-86.
- [25] Cochran KB, Dodds RH, Hjelmstad KD. The role of strain ratcheting and mesh refinement in finite element analyses of plasticity induced crack closure. *Int J Fat* 2011;33:1205-20.
- [26] Silitonga S, Maljaars J, Soetens F, Snijder HH. Numerical simulation of fatigue crack growth rate and crack retardation due to an overload using a cohesive zone model. *Adv Mat Res* 2014;891-892:777-83
- [27] Voormeeren LO, Van der Meer FP, Maljaars J, Sluys LJ. A new method for fatigue life prediction based on the Thick Level Set approach. *Engineering Fracture Mechanics* 2017;182:449-66.

- [28] Zerres P, Vormwald M. Finite element based simulation of fatigue crack growth with a focus on elastic-plastic material behaviour. *Comp Mater Sci* 2012;57:73-9.
- [29] Fischlschweiger M, Ecker W, Pippan R. Verification of a continuum mechanical explanation of plasticity-induced crack closure under plane strain conditions by means of finite element analysis. *Eng Fract Mech* 2012;96:762-5.
- [30] Jingjie C, Yi H, Leilei D, Yugang L. A new method for cyclic crack-tip plastic zone size determination under cyclic tensile load. *Eng Fract Mech* 2014;126:141-54.
- [31] Solanki K, Daniewicz SR, Newman JrJC. Finite element analysis of plasticity-induced crack closure: an overview. *Eng Fract Mech* 2004;71:149-71.
- [32] Jiang Y, Feng M, Ding F. A re-examination of plasticity-induced crack closure in fatigue crack propagation. *Int J Plasticity* 2005;21:1720-40.
- [33] Antunes FV, Rodrigues DM. Numerical simulation of plasticity induced crack closure: Identification and discussion of parameters. *Eng Fract Mech* 2008;75:3101-20.
- [34] Rodrigues DM, Antunes FV. Finite element simulation of plasticity induced crack closure with different material constitutive models. *Eng Fract Mech* 2009;76:1215-30.
- [35] Newman JC Jr. A finite element analysis of fatigue crack closure. Mechanisms of crack growth. ASTM STP 590; 1976.
- [36] Ellyin F, Wu J. A numerical investigation on the effect of an overload on fatigue crack opening and closure behaviour. *Fatigue Fract Engng Mater Struct* 1999;22:835-47.
- [37] Roychowdhury S, Dodds Jr RH. A numerical investigation of 3D small-scale yielding fatigue crack growth. *Eng Fract Mech* 2003;70:2263-83.
- [38] Antunes FV, Camas D, Correia L, Branco R. Finite element meshes for optimal modelling of plasticity induced crack closure. *Eng Fract Mech* 2015;142:184-200.
- [39] Salvati E, Zhang H, Fong KS et al. Separating plasticity-induced closure and residual stress contributions to fatigue crack retardation following an overload. *J Mech Phys Solids* 2017;98:222-35.
- [40] Smith KV. Application of the dissipated energy criterion to predict fatigue crack growth of Type 304 stainless steel following a tensile overload. *Eng Fract Mech* 2011;78:3183-95.
- [41] Sander M, Richard HA. Finite element analysis of fatigue crack growth with interspersed mode I and mixed mode overloads. *Int J Fatigue* 2005;27:905-13.
- [42] Pommier S, Freitas M. Effect on fatigue crack growth of interactions between overloads. *Fatigue Fract Engng Mater Struct* 2002;25:709-22.
- [43] Ellyin F, Ozah F. The effect of material model in describing mechanism of plasticity-induced crack closure under variable cyclic loading. *Int J Fract* 2007;143:15-33.

- [44] Pommier S. Cyclic plasticity and variable amplitude fatigue. *Int J Fatigue* 2003;25:983–97.
- [45] Borrego LP, Ferreira JM, Pinho da Cruz JM, Costa JM. Evaluation of overload effects on fatigue crack growth and closure. *Eng Fract Mech* 2003;70:1379-97.
- [46] Borrego LP, Antunes FV, Costa JD, Ferreira JM. Numerical simulation of plasticity induced crack closure under overloads and high-low blocks. *Eng Fract Mech* 2012;95:57-71.
- [47] Maljaars J, Pijpers R, Slot H. Load sequence effects in fatigue crack growth of thick-walled welded C-Mn steel members. *Int J Fatigue* 2015;79:10-24.
- [48] Chaboche JL. Time independent constitutive theories for cyclic plasticity. *Int J Plast* 1986;2:149-88.
- [49] Nip KH, Gardner L, Davies CM, Elghazouli AY. Extremely low cycle fatigue tests on structural carbon steel and stainless steel. *J Constr Steel Res* 2010;66:96-110.
- [50] Hodapp D, Collette M, Troesch A. Nonlinear fatigue crack growth predictions for simple specimens subject to time-dependent ship structural loading sequences. *Trans Soc Naval Architects and Marine Eng* 2013;121:57–90.
- [51] Willenborg J, Engle RM, Wood HA. A crack growth retardation model using an effective stress concept. Wright-Patterson: Air Force Flight Dynamics Laboratory; 1971.
- [52] Ray A, Patankar R. Fatigue crack growth under variable amplitude loading: Part I – Model formulation in state-space setting. *Appl Math Model* 2001;25:979–94.
- [53] Kurihara M, Katoh A, Kawahara M. Effects of stress ratio and step loading on fatigue crack propagation rate. In: Current research on fatigue cracks (Current *Japanese Materials Research*). London: Elsevier; 1987.
- [54] Overbeeke JL, De Back J. The influence of stress relieving and R-ratio on the fatigue of welding joints. In: Maccos SJ, editor. *Fatigue of welded constructions*, Brighton: The Welding Institute; 1987, p. 11–22.
- [55] Iwasaki T, Katoh A, Kawahara M. Fatigue crack growth under random loading. *Naval Arch Ocean Eng. (Jpn)* 1982;20:194–216.
- [56] Elber W. Fatigue Crack Closure under Cyclic Tension. *Eng Fract Mech* 1970;2:37–45.
- [57] Schijve J. Fatigue Crack Closure: Observations and Technical Significance, In: *Mechanics of Fatigue Crack Closure*, ASTM STP 982; 1988, p. 5–34.
- [58] Tada H, Paris PC, Irwin GR. *The stress analysis of cracks handbook*. 2nd ed. St Louis: Paris Productions Inc.; 1973.
- [59] Lee SY, Huang E-W, Woo W et al. Dynamic Strain Evolution around a Crack Tip under Steady- and Overloaded-Fatigue Conditions. *Metals* 2015;5:2109-2118.

- [60] Ding Z, Wang X, Gao Z, Bao S. An experimental investigation and prediction of fatigue crack growth under overload/underload in Q345R steel. *Int J Fatigue* 2017;98:155–166.
- [61] Schijve J. Effect of load sequences on crack propagation under random and program loading. *Eng Fract Mech* 1973;5:269–280.
- [62] Tanaka K. Mechanics and micromechanics of fatigue crack propagation. *Fracture Mechanics: Perspectives and Directions (Twentieth Symposium)*. ASTM Int 1989.
- [63] Yu, M., Chen, W., Kania, R., Boven, G. V., & Been, J. Underload-induced crack growth behaviour of minor cycles of pipeline steel in near-neutral pH environment. *Fatigue Fract Eng Mat Struct* 2015;38:681–692.